10

On the Mechanism of Laser Sintering of Polymer Structures Using Water

© E.D. Minaeva[1], N.V. Minaev[1], T.N. Popyrina[2], T.S. Demina[2], S.A. Gonchukov[3,4], O.L. Zakharkina[1], N.Yu. Ignateva[5], V.I. Yusupov[1]

[1] Institute of Photon Technologies of the Kurchatov Institute Research Center „Kurchatov Institute“, Moscow, Russia
[2] Moscow Aviation Institute (MAI), Moscow, Russia
[3] National Research Nuclear University „MEPhI“, Moscow, Russia
[4] Lebedev Physical Institute, Russian Academy of Sciences, Moscow, Russia
[5] Department of Chemistry, Moscow State University, Moscow, Russia

e-mail: minaeva.e.d@bk.ru

Received April 29, 2025
Revised June 19, 2025
Accepted October 24, 2025

Temperature fields and microstructural features of microparticles and structures made from them were investigated using thermography. Significant underestimation of instrument readings was revealed near the polymer melting temperature and in the area of laser spot impact. Structure formation depends on the composition of microparticles and laser exposure conditions. The most reproducible sintering result is observed for moistened microparticles with chitosan. The obtained results are collectively important for the development and optimization of technologies for synthesizing polymer powders and forming three-dimensional structures from them using laser additive technologies.

Keywords: thermal fields, laser sintering, DSC, thermography.

DOI: 10.61011/EOS.2025.10.62556.7865-25

Introduction

Three-dimensional constructs from polymer microparticles, formed by surface-selective laser sintering (SSLS), are used in electronics (filters, sensors), medicine (drug delivery, tissue engineering), and biotechnology (biocompatible materials) [1–3]. Recently, an approach using $\lambda = 1.96\,\mu$m radiation and water as a heating sensitizer has been developed [4]. It is assumed that the formation of three-dimensional constructs via SSLS occurs due to structural changes only in the surface layer of microparticles because of high absorption of radiation by water and low absorption by the polymer [4,5]. However, the understanding of the SSLS mechanism, including with water as a sensitizer, is currently lacking. In particular, it is unclear how melting of polymer microparticles can occur, given that their material has a very low absorption coefficient for laser radiation. Additionally, thermographic studies have shown that during sintering both with and without water, heating does not reach the polymer melting temperature or even the water boiling temperature [6].

The aim of this study is to clarify the mechanism of laser sintering of polymer structures, including those conducted in SSLS mode with water as a heating sensitizer, using multispectral thermography and numerical modeling.

Materials and methods

Polylactide (PLA) of the *Natureworks 4043D* brand (USA) (MM 100 kDa, $T_m = 155-160\,^\circ$C and $T_g = 55-60\,^\circ$C) was used in the work. PLA was ground in a mechanical mill at $T = -22\,^\circ$C and the target fraction with particle size $< 100\,\mu$m was selected using a sieve. Some particles were coated with a layer of chitosan (MM 80,kDa, degree of deacetylation 0.85) according to [5]. Characterization of microparticles was performed using an optical 3*D* microscope HRM-300 Series (Huvitz, Korea).

SSLS of structures was carried out on a setup consisting of a continuous Tm-laser ($\lambda = 1.96\,\mu$m, $P = 3$ W), an optical system with a galvanoscanner, and a system for forming layers of powdered material [5]. The laser spot diameter with Gaussian intensity distribution was $280\,\mu$m. Water was applied using an ultrasonic humidifier XA0065 (*Diymore*, China). Single-layer constructs in the form of a 6,mm diameter disk were formed in a 1 mm thick layer of microparticles at laser spot speeds of $v = 15$, 25 or 50 mm/s with a density of $12\,\text{mm}^{-1}$. Structures were formed from original/chitosan-coated polymer microparticles with and without humidification.

Thermography was performed using a FLIR A600 thermal imager (FLIR Systems, USA) (registration range $8-11\,\mu$m, frame rate 100 Hz) and an IRTS thermograph (IRTS, Russia) ($3-5\,\mu$m, 2 Hz). Calibration of the instruments was carried out using a copper heater with a 1 mm thick sapphire plate and a needle thermocouple with a diameter of $100\,\mu$m placed in the top layer of polymer microparticles (Fig. 1), which was applied to the plate surface. Calibration included the following steps: 1) temperature setting, 2) holding, 3) temperature recording using thermographs and the needle thermocouple. Note that when recording relatively high temperatures of

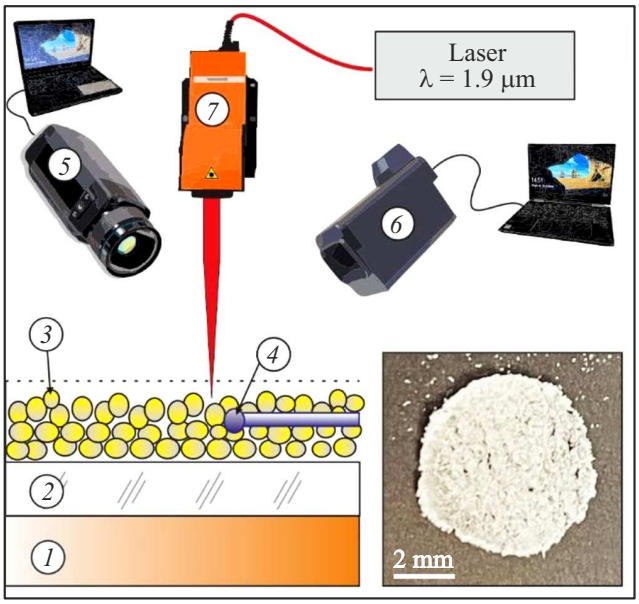

Figure 1. Schematic of the calibration stand on the SSLS setup: *1* — copper heater, *2* — sapphire plate, *3* — polymer material microparticles, *4* — needle thermocouple, *5* — FLIR thermal imaging camera, *6* — IRTS thermograph, *7* — galvanoscanner. The inset shows an image of the sintered structure.

polymer microparticles compared to the room temperature of surrounding objects, the influence of re-reflection of external temperature fields can be neglected.

Investigation of the microstructure of constructs was performed using a scanning electron microscope *PHENOM ProX* (*Phenom World*, Netherlands). For this purpose, constructs were embedded in epoxy resin, and cross-sections with a thickness of $300\,\mu$m were obtained using a *Leica* EM UC7 microtome (Germany). To assess the degree of heating impact on microparticles during laser sintering, differential scanning calorimetry (DSC) was used with a *Phoenix* DSC 204 calorimeter (*Netzsch*, Germany) at a heating rate of 10,K/min. Temperature field modeling was performed using *Matlab Laser Toolbox* [7].. Calculations utilized data on the fraction of absorbed $\lambda = 1.94\,\mu$m laser radiation in a polylactide microparticle layer ($\sim 32\,\%$) and the fraction of reflected radiation from such a layer ($\sim 40\,\%$) from [8]. All results are presented as mean and standard deviation. For comparing samples, the nonparametric Mann-Whitney U-test was used. Differences were considered significant at $p < 0.05$.

Results and Discussion

Investigation of original microparticles using an optical microscope showed that their size is $64 \pm 23\,\mu$m. PLA particles in transmitted and reflected light stood out distinctly as bright glowing areas. The latter indicates possible presence of microinhomogeneities scattering incident light. At the same time, in dark-field images of polymer particle cross-sections, only their contours are highlighted by light pixels, indicating that microinhomogeneities predominate exclusively on the surface rather than in the particle volume. It is precisely the presence of such microinhomogeneities and high light scattering on them that can explain the heating mechanism of original microparticles despite the low laser radiation absorption coefficient of the PLA material.

Calibration experiments demonstrated that errors in measuring the temperature of microparticles using the thermal imager and thermograph substantially depend on the „real“ temperature T_{real} controlled by the needle thermocouple (Fig. 2, *a*). In the range from 50 to 160 °C both instruments show lower temperatures compared to T_{real}. At $T_{\text{real}} = 160\,^{\circ}$C this difference amounts to $12 \pm 4\,^{\circ}$C and $28 \pm 6\,^{\circ}$C for FLIR and IRTS, respectively. The obtained dependencies are likely due to changes in the microstructure of the polymer particle layer. e believe that the local maximum is associated with „cold crystallization“ processes observed in DSC (Fig. 2, *b*), while the sharp drop in values in the 160 °C region is due to polymer melting. In the insets of Fig. 2, *a* it can be seen that at $T_{\text{real}} \sim 160\,^{\circ}$C the polymer layer has melted and become transparent from white.

DSC revealed a decrease in the enthalpy of relaxation and melting of polylactide in constructs, indicating that the polymer structure in constructs becomes closer to the equilibrium amorphous phase. Likely, laser exposure in the $v = 15$ mm/s mode ($F = 22\,\text{J/cm}^2$) and above causes melting of microparticles throughout their volume rather than surface sintering.

From Fig. 3, it is evident that single-layer sintered structures form in all modes. At $v = 15$ and 50,mm/s, the smallest thicknesses are recorded for original particles with and without humidification, while the largest are for humidified particles with chitosan. Interestingly, for the latter, structure thicknesses do not depend on the speed v.

Fig. 4 shows temperature profiles along tracks during SSLS. Regardless of particle type and presence of humidification, several characteristic sections can be distinguished on the curves. In the track start region, temperature rises rapidly, after which its growth slows down until approaching the laser spot, where another sharp rise is observed, followed by a rapid decrease. The curves record significant temperature fluctuations that intensify when approaching the laser spot. The profiles differ little from each other at constant laser spot speed. The most noticeable changes occur when varying the speed v: with its increase, the curves gradually approach the horizontal axis.

The modeling results for temperature distribution during laser exposure agree with the experimental data (Fig. 4). The largest deviations are observed in the laser spot area due to the limited resolution of the thermo-recording equipment, and for the IRTS thermographs also due to the low frame rate. Estimates show that low spatial resolution leads to the measured maximum temperature near the optical axis for FLIR being 0.7 ± 0.1 from the value that would be recorded at high resolution. For IRTS, this value is even lower at 0.2 ± 0.1.

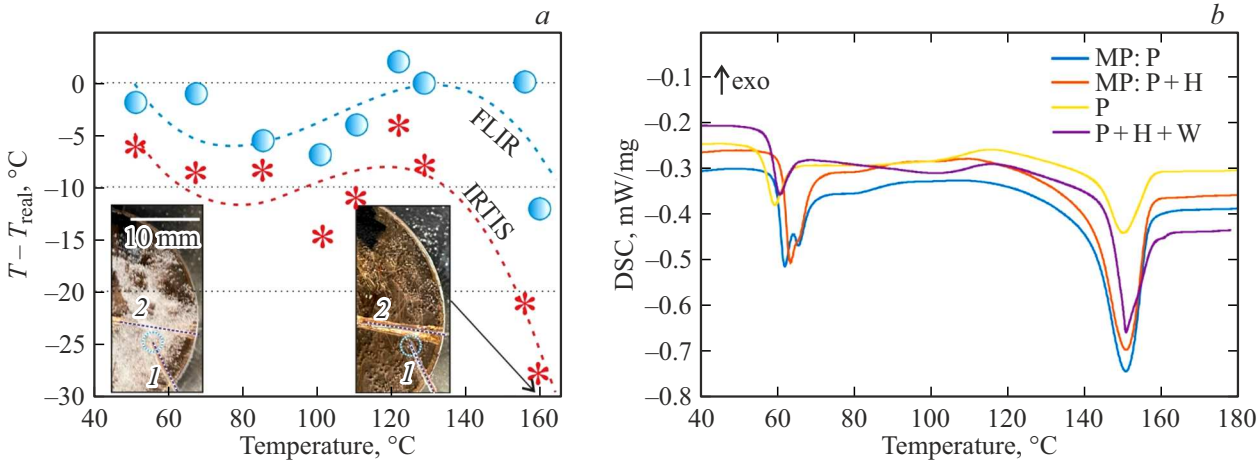

Figure 2. (*a*) Difference between temperatures of the surface layer of polymer microparticles measured by thermographs and thermocouple (T_{real}) with cubic trends. The insets show parts of the heater with the microparticle layer at $T_{real} = 40\,^{\circ}C$ and $160\,^{\circ}C$. *1* — thermocouple, *2* — built-in disk thermocouple. (*b*/) DSC for original microparticles (mp: P) and with chitosan (mp: P+H), as well as for structures ($v = 15$ mm/s) from original microparticles (P) and moistened microparticles with chitosan (P+H+W).

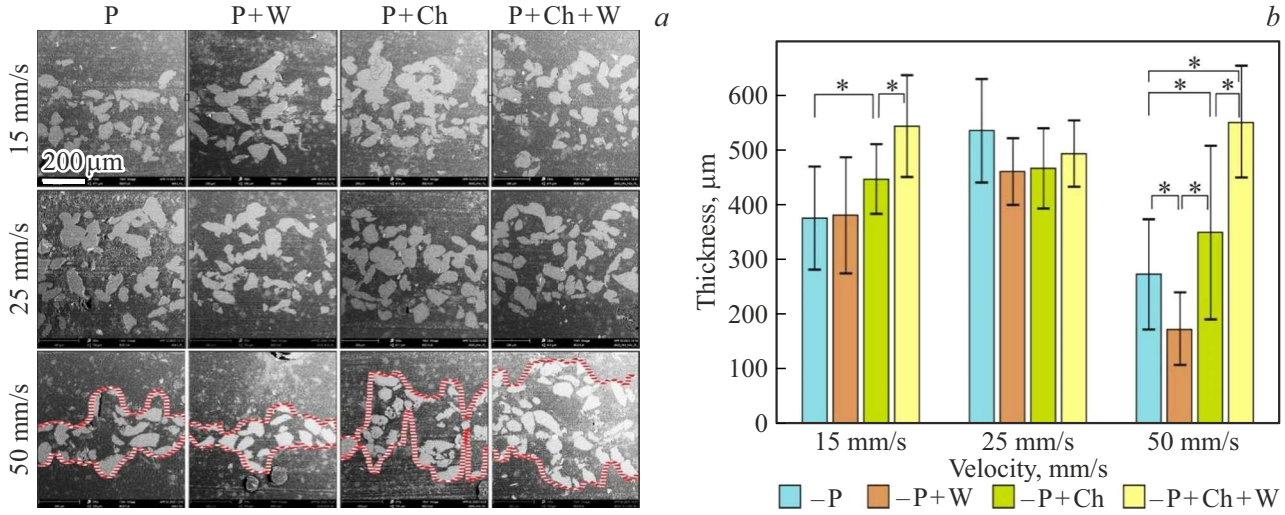

Figure 3. Characterization of obtained single-layer structures from various polymer microparticles in different modes. (*a*) SEM images of cross-sections. Red dotted lines highlight the upper and lower boundaries of structures obtained from image processing. (*b*) Dependence of single-layer structure thicknesses on the material used and water treatment: P — polymer, P+W — polymer+water, P+Ch — polymer+chitosan, P+Ch+W — polymer+chitosan+water.

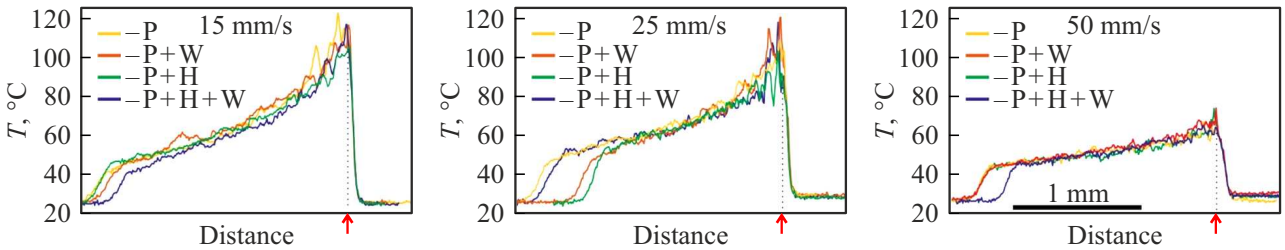

Figure 4. Temperature profiles along tracks in the plane of the optical axis during SSLS according to FLIR data. Designations as in Fig. 3. The position of the optical axis is marked by a red arrow. Decoding of designations P, P+W, P+H, P+H+W is given in Fig. 3.

Conclusion

Calibration measurements showed that thermo-recording equipment can substantially underestimate the temperature of the microparticle surface layer, especially when approaching the polymer melting temperature. At the same time, thermography data obtained with the FLIR thermal imager can be used to analyze temperature distribution, except in the laser spot area. Characteristics of sintered structures depend on particle composition and processing conditions, with the most reproducible sintering result observed for humidified microparticles coated with chitosan. In the laser sintering mechanism, an important role belongs to the microstructure of the microparticle surface, which affects optical properties. The research results can be used to optimize the SSLS additive technology.

Funding

This work was carried out within the state assignment NRC Kurchatov Institute.

Conflict of interest

The authors declare that they have no conflict of interest.

References

[1] W. Han, L. Kong, M. Xu. International J. Extreme Manufacturing, **4** (4), 042002 (2022). DOI: 10.1088/2631-7990/ac9096
[2] H.M. Yehia, A. Hamada, T.A. Sebaey, W. Abd-Elaziem. J. Manufacturing and Materials Processing, **8** (5), 197 (2024). DOI: 10.3390/jmmp8050197
[3] Y.A. Gueche, N.M. Sanchez-Ballester, S. Cailleaux, B. Bataille, I. Soulairol. Pharmaceutics, **13** (8), 1212 (2021). DOI: 10.3390/pharmaceutics13081212
[4] V.N. Bagratashvili, E.N. Antonov, V.K. Popov, V.I. Yusupov. Patent №150514. 20.02.2015. (in Russian) Byull. No.5.
[5] N.V. Minaev, T.S. Demina, S.A. Minaeva, A.A. Dulyasova, E.D. Minaeva, S.A. Gonchukov, T.A. Akopova, P.S. Timashev. Izv. RAN. Ser. Fiz., **11** (1530-6), 2020 (in Russian). DOI: 10.3103/S1062873820110192
[6] E.D. Minaeva.
it Lazerno-inducirovannoe formirovanie biosovmestimyh konstrukcij iz polimernyh materialov i lazernaya biopechat' kletochnymi agregatami dlya tkanevoj inzhenerii. Avtoref. kand. dis. NIYAU MIFI, M., 2024 (in Russian).
[7] I. Hernando, M.A. Renderos, M. Cortina, J.E. Ruiz, J.I. Arrizubieta, A. Lamikiz. In: *Procedia CIRP (LANE 2018)*. (Elsevier, 2018) vol. 74, p. 674–678. DOI: 10.1016/j.procir.2018.08.045
[8] G.R.B.E. Römer, A.J. Huis in't Veld. In: *Physics Procedia* (*6th International Conference on Laser Assisted Net Shape Engineering*), (Elsevier, 2010) vol. 5 (Part B), p. 413–419. DOI: 10.1016/j.phpro.2010.08.068

Translated by J.Savelyeva